DYNAMIC MASKING TECHNIQUES FOR PARTICLE IMAGE VELOCIMETRY

F. Gökhan ERGİN
Dantec Dynamics A/S
Tonsbakken 16-18, 2740, Skovlunde, Denmark, gokhan.ergin@dantecdynamics.com

Abstract: Objects and surfaces often appear in Particle Image Velocimetry (PIV) images. Unless masked, the features on these contribute to the cross correlation function and introduce an error in the vectors as a result of the PIV analysis in the vicinity of the phase boundary. Digital masking of objects has appeared numerous times in the literature as part of the analysis chain, with a growing focus on isolating moving features using dynamic masks. One aim of this article is to provide a summary of milestones achieved in dynamic masking covering a wide range of applications. Another aim is to show the difference between image masking and vector masking. Finally, two different dynamic masking examples are described in detail and compared. The examples used are selected from swimming microorganisms in small channels. In the first example, a histogram thresholding-based dynamic masking is used, while, in the second example, a novel technique employing a feature tracking-based dynamic masking is used. Results show that histogram thresholding-based masking provides better results for swimmers which randomly change shape and direction; whereas, feature tracking-based masking provides better results for swimmers which do not change shape or direction significantly. In order to show the improvement due to dynamic masking, a comparison is made between PIV results a) with no masking, b) with just image masking and c) with both image and vector masking. Results show that the best approach is to use both image and vector masking.
Keywords: Dynamic masking, Image masking, Vector masking, Histogram thresholding based dynamic masking, Feature tracking-based dynamic masking.

PARÇACIK GÖRÜNTÜLEMELİ HIZ ÖLÇME TEKNİĞİ İÇİN DİNAMİK MASKELEME TEKNİKLERİ

Özet: Cisimlere ve yüzeylere Parçacık Görüntülemeli Hız Ölçümü (PIV) imajlarında sıkça rastlanır. Bunlar maskelenmediği sürece, çapraz korelasyon fonksiyonunu etkiler ve PIV analizi sonucu elde edilen hız vektörlerinde faz sınırına yakın yerlerde hatalı sonuçlar oluşturur. Cisimlerin dijital ortamda maskelenmesi, özellikle hareketli cisimlerin dinamik maske kullanılarak imajlardan çıkarılması hesap zincirinin bir parçası olarak literatürde pek çok kez yayınlanmıştır. Bu yazının bir amacı dinamik maskelemede ulaşılan kilometre taşlarının geniş bir uygulama yelpazesini de kapsayan bir özetini vermektir. Bir diğer amaç ise dinamik imaj ve vektör maskelemenin farklarını göstermektir. En son olarak, iki ayrı dinamik maskeleme örneği ayrıntılı olarak anlatılmakta ve karşılaştırılmaktadır. Kullanılan örnekler küçük kanallarda yüzen mikroorganizmalardan seçilmiştir. İlk örnekte histogram eşikleme ile dinamik maskeleme ve ikincide ise yeni bir teknik olan, özellik takibi ile dinamik maskeleme kullanılmıştır. Sonuçta, histogram eşikleme ile maskelemenin yüzme yönü ve şekli rastgele değişen yüzücülerde; özellik takibi ile maskelemenin ise şekli ve yönü pek değişmeyen yüzücülerde daha iyi sonuçlar verdiği ortaya çıkmaktadır. Dinamik maskelemenin yararını göstermek için maskeleme yapılmadan elde edilmiş PIV sonuçları, sadece imaj maskelemesi yapılarak elde edilmiş PIV sonuçları ve hem imaj hem de vektör maskelemesi yapılarak elde edilmiş PIV sonuçları karşılaştırılmıştır. Sonuçta hem imaj hem de vektör maskelemesinin kullanılmasının daha uygun olduğu ortaya çıkmıştır.
Anahtar Kelimeler: Dinamik maskeleme, İmaj maskeleme, Vektör maskeleme, Histogram eşikleme ile dinamik maskeleme, Özellik takibi ile dinamik maskeleme.

INTRODUCTION

Masking is an important step during PIV processing and, in many cases, manually-drawn static masks are sufficient to remove stationary objects from PIV images. Masking can be a relatively easy process if the unwanted section or object is stationary, however, it becomes an extremely cumbersome and time-consuming process if the object is moving. Especially in the case of time resolved PIV systems,—where thousands of images can be acquired in an image ensemble—manual masking of moving objects from each image is simply not practical. Static digital masking is rather straightforward and has appeared numerous times in the PIV literature;

therefore, any reference to static masking techniques is omitted here, and the focus will be on dynamic masking.

With the introduction of high-speed PIV systems, time-resolved flow field information has become more readily available. Along with generating large numbers of images, this has also driven a necessity for an effective dynamic masking process when phase separated image processing is required in various multi-phase flow investigations. There are often significant velocity gradients across phase boundaries, which can cause cross-correlation based PIV methods to fail. Ironically, phase boundaries are often the focus of investigations where important fluid dynamics phenomena occur. In interrogation windows which overlap the boundary, the PIV computations are more likely to represent the displacements of the phase with the greater density of particle images. Therefore, it is essential to identify the phase boundary accurately in order to perform phase-separated PIV evaluations for a more accurate representation of the flow field where interesting flow phenomena occur.

To date, many multi-phase flow investigations have used some form of dynamic masking and these cover almost all phase combinations: gas in liquid (e.g. bubbly flow reactors, boiling flows), liquid in gas (e.g. sprays, free surface flows), liquid in liquid (e.g. droplet formation, mixing), gas in gas (e.g. combustion diagnostics, flame front investigations), solid in liquid (e.g. sediment transport, swimming objects), solid in gas (e.g. flapping and flying objects) and solid, liquid and gas (e.g. landslide investigations). Separation of phases can be accomplished using optical methods, digital methods, and using additional hardware components (e.g. a secondary illumination mode, Lindken and Merzkirch, 2002). Phase separation can, of course, also be achieved using a combination of these. Of particular interest—and the focus of the current report—are the digital methods which create dynamic masks of moving objects by applying a number of image processing functions using the original image ensemble. Although a number of different image processing techniques can be used in tandem, digital separation methods can be grouped under three main categories: (i) size-based separation, (ii) greyscale histogram thresholding methods and (iii) boundary detection methods. This study is a first attempt to summarize existing literature on the three digital separation methods. Additionally, two examples are provided of recent dynamic masking applications from bio-micro-fluidics. The first application example demonstrates masking of a uniflagellate microorganism using histogram thresholding and the second details masking of a copepod microorganism using a novel feature tracking-based approach.

Size-based separation

The *first study* using moving masks for phase-separated PIV processing was by Gui and Merzkirch (1996) in a bubbly flow experiment. In their analysis, a digital mask was used to track & separate larger gas phase objects (bubbles) from the smaller seeding particles in the liquid phase for double-frame PIV recordings. The separation technique relied on the existence of a significant difference in size distribution between the bubbles and the seeding particles. In another bubbly flow investigation from the same research group, Lindken and Merzkirch (2000) used a similar digital masking technique. In this study, a secondary high-speed imaging system was added to reconstruct the bubble shape and position in three-dimensions. The light sheets of the two systems were perpendicular to one another, and the 3D bubble shapes were reconstructed using the 2D bubble contours produced by each of the high-speed imaging systems. The use of this secondary imaging system allowed phase-separated *measurements of simultaneous, multiparameter information*: (i) two-component planar velocity field, (ii) bubble positions and (iii) 3D bubble shapes.

Separation of three phases was achieved by Fritz et al. (2003), who performed digital dynamic masking in a landslide wave tank without using additional hardware components. First, the seeding particles in the water phase were separated from the sliding granular matter and air, using image-processing functions. Second, the pixel value fluctuations arising from illumination intensity were removed using a sliding background subtraction. Finally, the water phase was isolated from the other two phases using digital dynamic masks similar to techniques used in Lindken & Merzkirch (2000). The ramp and water surface were masked to avoid biased correlation signals caused by total reflections and light scattering from floating seeding particles. This masking technique was used successfully in un-separated and separated flow conditions, meaning the mask was able to follow *morphological changes* in the two-phase flow.

The size-based separation methods naturally rely on a significant size difference between the phases. If the size difference is small, i.e. if the size of the bubbles are close to the size of the particles, phase separation becomes quite difficult. Histogram thresholding methods, in combination with other image processing functions, have certain advantages in such situations and can be more effective when applied to other challenging flow configurations.

Histogram thresholding methods

Lindken and Merzkirch (2002) improved upon their previous size-based separation method by adding a histogram thresholding-based separation approach. They used the digital mask as an operator in the PIV

evaluation algorithm in which the separation of phases is performed on individual image histograms. Furthermore, a *secondary light source* in transmission mode was used in combination with PIV in order to get distinct background levels between particles and bubble areas. The detailed image processing steps are implemented such that they can be applied to large image ensembles in a systematic fashion (*automated masking*).

In the realm of PIV literature, the term "dynamic masking" was first coined by Sveen and Daziel (2005). In their approach, dynamic masking allowed *simultaneous measurements of velocity and density gradients* by separating PIV and synthetic Schlieren signals in a gravity wave tank. In the experiment, backlit particle shadows were superimposed on synthetic schlieren images. The particle images were removed using a 3-step masking procedure. First, a background subtraction was performed based on pixel maximum to remove static features on the tank walls. Second, a histogram thresholding was performed to locate the particles, and third, an erosion filter was applied to increase the imaged particle size. The resulting image was used for masking the synthetic Schlieren images. Sveen and Daziel (2005) even measured the performance of their dynamic masking technique by comparing the RMS signal of a) a non-seeded measurement, b) a seeded measurement without a mask and c) the seeded measurement with dynamic masking. They observed that the masking technique reduces RMS errors by 7%.

Another performance assessment was made by Seol & Socolofsky (2008) using a PIV/LIF (Laser Induced Fluorescence) experimental setup. In this study, experiments were performed in a bubbly two-phase flow and made a *three-way comparison* between a) optical phase separation, b) digital phase separation (masking) and c) mixed-phase PIV analysis with vector post processing. As a result of the error analysis among the data sets, it was found that the vector post-processing algorithm performed well, but contained small errors in the fluid-phase velocity field around some bubbles. A five-step image processing chain was used to identify the bubble signatures for masking: (i) a 3x3 median filter, (ii) histogram thresholding at 5% of peak pixel value, (iii) binarization, (iv) opening / closing filters and (v) a dilation filter were used to generate the masking algorithm. The binary image mask was then multiplied by the original image to separate the bubbles from the fluorescent particles. In the processed particle image, *the missing* bubble *regions were filled with an average background pixel value* instead of a zero-pixel value so that the PIV algorithm is not biased by the sharp edges created by the masked bubble regions.

Up until 2010, all the histogram thresholding-based techniques used in bubbly flow experiments relied on the use of additional systems or hardware components. In 2010, Deen et al. (2010) and Hammad (2010) reported masking of stationary and moving objects using only image processing functions, i.e. *without the use of additional hardware components*. Deen et al. (2010) described a combined image processing approach that deals with uneven illumination and masking, where a two-phase flow between the filaments of a spiral wound membrane module was digitally separated. The approach consisted of (i) intensity normalization to cope with uneven illumination, (ii) background subtraction to remove stationary objects and (iii) image masking to remove the moving bubbles in two-phase flow. The removal technique of moving bubbles—which appear as bright rings on the image—was similar to what was developed by Seol & Socolofsky (2008). Hammad (2010) performed phase-separated velocity measurements in a two-phase flow experiment in which the turbulent bubbly flow was produced by an impinging water jet on a horizontal air-water interface. Dynamic masking was performed using a sequence of low-pass, high-pass and morphology digital filters to yield background subtraction, bubble detection and phase separation. The liquid-phase containing the seeding particles was produced first by identifying the areas occupied by bubbles using median filtering, and then by subtracting the bubbles from contrast-enhanced images. Each phase was evaluated separately using an adaptive correlation-based PIV algorithm.

In general, the dynamic masks generated in the literature have been accurate down to a single pixel. Wosnik and Arndt (2013) applied a slightly different dynamic masking technique based on a *local threshold filter applied on the interrogation area*. The experiment was performed in a bubbly wake produced by ventilated supercavitation, where only the velocity fields of the gas phase in the cavitating flow were obtained by PIV analysis of the bubbles. In order to retain vectors associated with bubbles, the original PIV image was thresholded not pixel-by-pixel, but by the size of the final interrogation area. The masked and unmasked regions were defined based on a pixel value summation over the final interrogation area compared to a defined threshold value. In other words, if the sum of the pixel values was above a certain threshold, the mask was "on", and if below the mask was "off". Therefore, the 1024x1024 original image was converted to a 63x63 binary image mask for 32x32-pixel final interrogation area and 50% overlap. That approach naturally produced a mask with coarser resolution.

Histogram thresholding-based dynamic masking has also been applied in other challenging applications. Among these are (i) the masking of organisms during locomotion, (ii) the masking of droplets during break-up and (iii) the masking of reactants and products in combustion diagnostics.

Wadhwa et al. (2014) used a dynamic masking algorithm to investigate the flow field around *A. Tonsa*, a sub-millimeter sized microorganism*, during locomotion*. A two-step masking procedure was applied to remove the organism from the particle images: The procedure consisted of a sliding averaging of the pixel intensity values followed by thresholding to remove those pixels from the analysis which corresponded to the organism. The masking process made it "impossible" to get measurements in the close vicinity of the organism, especially around the swimming appendages. As a result, the masking parameters had to be adjusted for each recording manually in order to minimize the loss of useful data. After every pass of the processing and during post-processing, outliers were removed using a median filter and de-noising. Later Ergin et al. (2015a) applied a feature tracking-based dynamic masking approach to achieve better results using the same raw images. This approach will be described in detail in Section 3.

Carrier et al. (2015) used dynamic image and vector masking successfully in a droplet formation experiment where the dynamic mask was used to reject spurious vectors in the non-seeded continuous phase. The first step was to isolate the features in motion (the droplet interface and the seeding particles) from the static background. For this purpose, the harmonic mean was subtracted from the inverted pixel values of the raw shadow images. In addition to this, a static mask was applied to remove residual wall reflections. Finally a suitable histogram threshold level was selected so that only the features in motion had a non-zero pixel value. Then a sufficient number of dilations (bright pixels flooding the dark pixels) were performed to fill the gaps between the particles and the interface entirely. A natural side effect of this dilation is the 'fattening' of the finger, which can be remedied by an equal number of erosions (dark pixels flooding the bright pixels). The masks generated in Carrier et al. (2015) were successful in following the *morphological changes during the droplet formation*, especially during the break-up stage (Fig. 1). A movie of the droplet break-up is available in Ref M1**.**
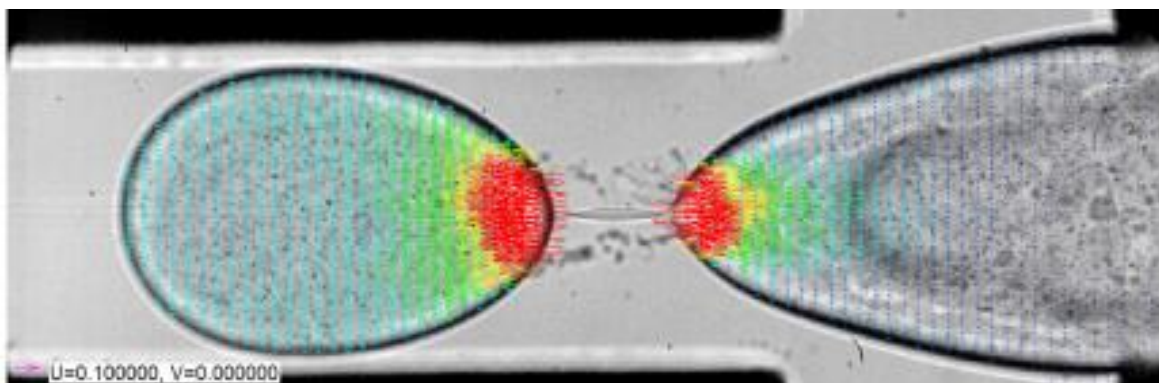
Stevens et al. (1998) performed *phase-separated PIV measurements in a combustion application*. The experiment consisted of a premixed turbulent methane-air flame in a stagnation plate configuration, where a dynamic masking technique was used to improve the PIV results for interrogation areas located along the flame front. In order to separate the reactant and product zones, local seeding density was used as the differentiator. The seeding density is often higher before combustion, and lower afterwards due to a sudden expansion of gases. As a result of the seeding denisty change, local mean pixel intensity in the PIV images is higher in the air-fuel mixture before combustion than after. Stevens et al. (1998) were able to determine the thin flame front using the Light Sheet Tomography technique, which is based on the local intensity of Mie scattering from the seeding particles. A suitable threshold applied on the mean pixel values was used to separate the two zones and a cross-correlation-based PIV algorithm was applied in each zone separately.

The histogram-thresholding techniques seem to be more frequently applied in the literature; particularly for the masking of multiple medium-sized features in the flow field, such as bubbles, microorganisms, and droplets. Due to their flexibility and their ability to handle more challenging situations, they can even produce successful results along more complex phase boundaries such as a flame front in combustion applications.

Boundary detection methods

Boundary detection methods are more suitable for separation of phases across longer, single-phase boundaries such as flame fronts, surface instabilities and liquid free surfaces. For example, Coron et al. (2004) used a boundary detection method for *phase separation in a turbulent premixed flame*, very similar to what is described by Stevens et al. (1998). Both groups were successful in (i) obtaining the phase-separated instantaneous velocity fields simultaneously, and (ii) improving the accuracy of the PIV measurements in the vicinity of the flame front. Additionally, Coron et al. (2004) were able to measure

Figure 1. Snapshot of the flow field at rupture instant during the droplet break-up experiment performed by Carrier et al. (2015). Colors indicate velocity magnitude, max velocity 270 mm/s. Histogram thresholding based dynamic mask is able to follow morphological changes during droplet formation.

the flame front contour location. Coron et al. (2004) also perform a phase separation between fuel and reactants based on the fact that Mie scattering light intensity from the seeding particles is lower in products than in reactants—due to the gas expansion across the flame front. In this study however, the active (deformable) contours technique was used for boundary detection rather than a histogram thresholding method. These deformable contours can be breifly described as curves or surfaces defined within a multi-dimensional domain which can move toward desired features (usually edges). The preferred model for their study employed parametric active contours, which allowed a compact representation of data. The boundary detection technique using active contours is an iterative procedure, in which an initial contour on the image domain is allowed to deform. Coron et al. (2004) used a contour obtained by the reliable averaging windows technique as an initial guess. After the final flame front contour was obtained, a mask was produced on one side of the contour at a time with PIV analysis performed in the fuel mixture phase and the combustion products phase separately. As a result, in regions where the interrogation windows stretch across the flame front, the densely seeded fuel phase did not influence the correlation function in the reactants phase.

Another application where boundary detection methods prove to be more suitable are flows with free liquid surfaces. Sanchis and Jensen (2011) used Radon transformation for automatic boundary detection and performed phase separation in a *stratified two-phase flow* through a circular pipe. The boundary was identified by the seeding particles floating at the free surface, which appeared as a long connected dotted line in PIV recordings. The Radon transform is a mathematical tool well suited for the detection of linear features in noisy images and is commonly applied in computer vision. This technique tends to suppress pixel intensity fluctuations due to noise by the process of integration. A normalization procedure was included to take into account the aspect ratio of rectangular input images. During image processing, segmentation was necessary and an increased number of image segments were used in areas with increased curvature. Hermite cubic interpolation between adjacent segments allowed the reconstruction of the interface piece by piece across the entire image. This technique was able to track the interface with an accuracy of +/- 0.67 pixels under worst-case scenarios; i.e. in low particle density and with a noisy background.

Honkanen and Saarenrinne (2003) provided a good overview of other digital object separation methods and their application in PIV analysis of turbulent bubbly flows. They described four different object separation methods including (i) probability of centre, (ii) convex perimeter, (iii) curvature profile and (iv) Shen's method. The last three are breakpoint detection methods and were found to be more efficient than the probability of centre method for bubbly flows. Their superior performance is due to the fact that they search for connecting points of outlines of individual objects on the perimeter of the segment. Among all four methods the curvature profile method located the connecting points most accurately and most reliably, and it was also the least sensitive to noise. It should be noted that these findings only apply for bubbly flows where smooth contours are normally encountered during PIV recording.

As can be seen in the literature, there are a great number of different masking approaches used by researchers, and it is quite difficult to universally comment whether one approach is better than the other. In the current work, the aim is not to name the best masking technique that works in every scenario. On the contrary, based on previous studies, the dynamic masking approach should be tailored for each application. Regardless of the approach being used, mask definition is the same; information from one or more phases must be suppressed while leaving information from the remaining phase(s). In the next section the mask definition for image masking and vector masking is presented.

Mask definition

The goal of dynamic masking is to get a specific pixel value (such as "0") on the object that is to be masked and retain the pixel value information everywhere else for each image in the ensemble. This can be achieved in a 3-step procedure. In step one; a new image ensemble is produced by filtering, thresholding etc. to obtain a pixel value of 0 on the object and 1 everywhere else (Gui and Merzkirch 1996). In step two, each time step of the new image ensemble is multiplied by the corresponding time step of the original ensemble. If the original image background pixel value is nonzero, this results in a sharp pixel value difference between the mask and the image background. As a remedy, in step three, background subtraction techniques can be used to obtain a 0 pixel value in the masked ensemble's background, or the masked area can be padded with the average pixel value of the background (Seol & Socolofsky 2008). Finally, the mask ensemble can be applied to mask either the raw images (image masking) and/or the PIV results (vector masking). In short, the preferred image masking definition here is following Gui and Merzkirch (1996), where the mask is defined as a binary image and it is applied on the raw images using pixel-by-pixel image multiplication:

Δ (i,j)= 0 if the pixel, p(i,j) belongs to the phase that is to be masked (Phase 1)

Δ (i,j)= 1 if the pixel, p(i,j) belongs to the phase that is subject to PIV evaluation (Phase 2).

A typical phase-separated PIV evaluation of a two-phase flow starts with image masking of phase 1 and PIV evaluation in phase 2. Then the binary mask is inverted to mask phase 2 using a simple pixel inversion and PIV evaluation is performed on phase 1. An additional vector masking step is usually applied after each evaluation in order to clean up the vectors in the masked phase close to the phase boundary (see Fig. 6). The vector masking definition is similar to image masking:

Δ (i,j)= 0 if the vector V(i,j) belongs to the phase that is to be masked (Phase 1)

Δ (i,j)= 1 if the vector V(i,j) belongs to the phase that is subject to PIV evaluation (Phase 2)

Finally, both vector maps are merged to represent the two-phase flow field. For multiphase flows where more than 2 phases are present, the same approach can be used a number of times until each phase is represented in the flow field. In some cases, one of the phases could be a solid boundary in motion (e.g. flapping wing, rotating vane etc.) where PIV evaluation may not be necessary. In the following two sections, different dynamic masking strategies are described using the above mask definition. In the Section 2, flow around a uniflagellate swimmer, *Euglena Gracilis* (*E. Gracilis*), is isolated using histogram thresholding-based dynamic masking. In the Section 3, flow around a breaststroke swimmer, *Acartia Tonsa* (*A. Tonsa*), is isolated using a novel tracking-based dynamic masking technique. Recently, similar dynamic masking procedures for *E. Gracilis* and *A. Tonsa* have been reported in Ergin (2015) and in Ergin et al. (2015a), respectively. The current work uses the same two raw particle image ensembles, but provides improved comparisons and descriptions (including flow charts for data analysis) of masking and velocimetry. In the case of *E. Gracilis*, the importance of dynamic masking is demonstrated by providing a three-way comparison between PIV results with a) no masking, b) image masking and c) vector masking. Similarly for *A. Tonsa*, a comparison between unmasked and masked PIV results is provided.

HISTOGRAM THRESHOLDING-BASED DYNAMIC MASKING

The microorganism *E. Gracilis* is known to use a single whip-like structure, called flagellum, in combination with rolling, stretching and contracting its flexible body. A schematic of this mono-flagellate is shown in Fig. 2. Its body length without the flagellum can vary between 20µm and 100µm. The flagellum is located at the end close to the photoreceptor, and the cell nucleus is centrally located in its body. Although imaging the flagellum is challenging, the photoreceptor and the cell nucleus can be detected easily under a microscope (Fig. 2).
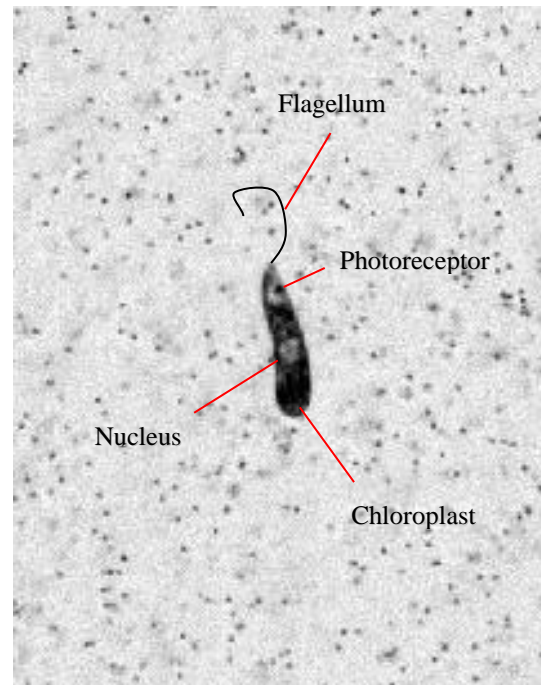

Figure 2. Schematic of *E. Gracilis*. Flagellum is added manually as it cannot be resolved by the optics. The photoreceptor, nucleus and chloroplast are visible under the microscope.

The experimental measurement setup used in this masking example is a MicroPIV system manufactured by Dantec Dynamics. The system components include an inverted fluoresence Microscope (HiPerformance), a sensitive CMOS detector (SpeedSense M310), a synchronization device (80N77 Timer Box), and a pulsed LED illumination system (Microstrobe). In biological flows, high-power pulsed laser illumination is often not preferred as this can disable the organism or influence its normal locomotion behaviour. For this reason, a lower-power LED-based pulsed illumination was used in backlit transmission mode which produced shadow particle images. 1µm-diameter seeding particles were introduced in small quantities until a sufficient seeding density was achieved for PIV. The seeding density was kept at a low level in order to avoid a change in normal swimming behaviour. The particle images were recorded at a frame rate of 12.5 fps, with a resolution of 1280 x 800 pixels. The images were acquired using a 40x magnification objective, producing a 0.64 mm x 0.4mm field of view (FoV). Later a smaller region of interest (ROI) is extracted with a resolution of 323 x 529 pixels, corresponding to 162µm x 265µm in the object space. Single-frame image acquisition was performed with a constant time difference of 80ms. Since the FoV was relatively small (~0,25mm^2), it was often necessary to wait until an organism swam through the FoV with the measurement system in operation. The images were continously acquired and stored in a ring buffer with the acquisition stopped manually after the organism had passed through the FoV. 83 consecutive frames were analyzed to produce 82 flow field measurements. Total recording time was 6.56s. Further details can be found in Ergin (2015).
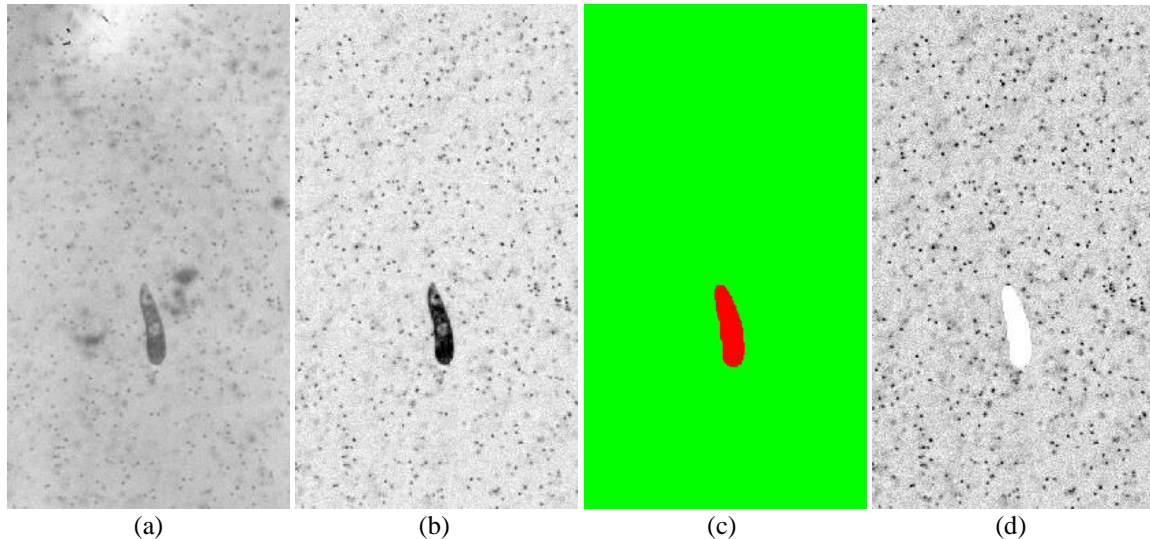
Figure 3. *E. Gracilis* during locomotion in water with 1-µm diameter seeding particles at t=1.92 s. (a) Raw image before background subtraction (b) after pixel inversion and background subtraction (re-inverted) (c) dynamic mask (d) particle image after image masking (re-inverted)

Fig. 3a shows the raw PIV recording of a 47,5µm-tall *E. Gracilis* in the sparsely seeded flow. In the acquired ensemble, *E. Gracilis* meanders upwards through filtered water; covering a net distance of approximately 256µm (Fig. 4). Use of filtered water provides a cleaner, foreign-object-free background in the raw images and allows more precise seeding density adjustments. Furthermore, other marine organisms (predator or prey to *E. Gracilis*) that can change *E. Gracilis*' normal locomotion behaviour are excluded.
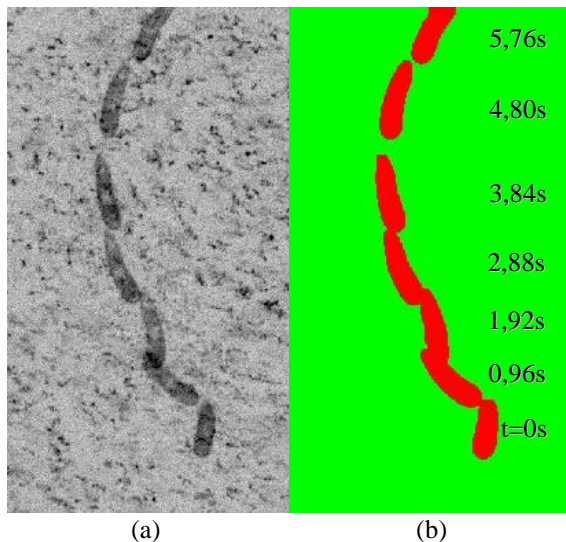

Figure 4. Quality of dynamic masking (a) Recorded position (b) dynamic mask of *E. Gracilis* every 0.96s.

The first step in image pre-processing is pixel inversion in order to work with positive particle images rather than particle shadows. Although working with (inverted) positive particle images during processing, it is preferable to present (re-inverted) shadow particle images for better visibility (Fig. 3b and 3d). In the second step, a background

subtraction is performed using the minimum pixel value found in the inverted ensemble (Fig. 3b). Next, a histogram thresholding-based dynamic mask is produced using the ensemble in the second step (Fig. 3c) and finally image masking is performed (Fig. 3d). A flow chart describing the complete analysis chain for dynamic masking of *E. Gracilis* is shown in Fig. 5.
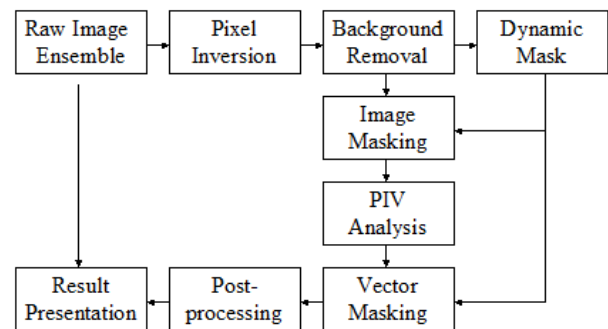

Figure 5. Flow chart describing the analysis chain for dynamic masking of *E. Gracilis*.

In the current study, the following image processing chain produced an acceptable dynamic mask: a 9x9 median filter, a closing filter with 10 iterations, thresholding (min:125 max:4096), pixel inversion, thresholding (min:3970 max:4096), erosion filter with 2 iterations, thresholding (min:0 max:1). The final thresholding step produces the binary image mask. In order to demonstrate the quality of the dynamic mask, position of *E. Gracilis* (Fig. 4a) and the used mask (Fig. 4b) are shown side by side at selected time steps. One immediate observation is that the mask is slightly larger than the organism. This is intentional in order to keep a small margin around the masked object, and the margin thickness can be controlled by the number of erosions and dilations. Another observation is that the used mask may produce non-ideal results around image boundaries (see for example the top of Fig. 4b at t=5,76s). Apart

from these, the dynamic mask captures the position and the shape of *E. Gracilis* in a successful fashion.

For velocity calculations, an adaptive PIV algorithm is used, which is an advanced particle displacement estimator implemented in DynamicStudio (Dantec Dynamics, Skovlunde, Denmark). Briefly, the implementation is a cross-correlation based, adaptive and iterative procedure employing vector validation and deforming windows: First, the displacement is calculated on an initial interrogation area (IA), which is larger in size compared to the final IA. In each step the IA is shifted by the displacement calculated in the previous step. For the case of *E. Gracilis* the final interrogation windows of 32x32 pixel are used with 75% overlap. Window deformation is performed by adapting the IA shape to velocity gradients, with $|du/dx|$, $|dv/dx|$, $|du/dy|$, $|dv/dy| < 0.25$.

Several passes can be made to further shift & deform the windows to minimize the in-plane particle dropout. For each IA size, this procedure is repeated until a convergence limit in pixels or a maximum number of iterations is reached. Then a 9-point, two-dimensional Gaussian fit is performed on the highest correlation peak to obtain the displacement field with subpixel accuracy in each pass. A number of FFT window (Hanning, Hamming etc.) and filter functions can be applied during the analysis. Between passes, spurious vectors are identified and replaced with a number of validation schemes including peak height, peak height ratio, SNR & Universal Outlier Detection (UOD) (Westerweel and Scarano 2005). Following Westerweel and Scarano (2005), UOD is performed between passes in a 5x5 neighbourhood with 0.1 minimum normalization level and a detection threshold of 2.0. The vectors are considered valid if the peak height ratio is larger than 1.25. In other words, the displacement calculation is considered reliable when the highest peak (the assumed signal peak) is at least 1.25 times higher than the second highest peak (assumed to be noise) in the cross-correlation function. This is certainly not the only vector validation method, but it is one of the oldest. A threshold value of 1.2 is often used in the literature, so in this respect the present threshold value of 1.25 is more conservative. The subpixel positioning accuracy of the Adaptive PIV algorithm is reported as 0.06 pixels with 95% confidence (Ergin et al. 2015b). The 0.06 pixels correspond to a 27.5nm displacement in the object space, and the velocity uncertainty is estimated as 0.34μm/s. An average filter in a 5x5 neighbourhood and vector masking is applied after Adaptive PIV computations.

A close up of the flow field around *E. Gracilis* at t=1.92s is shown in Fig. 6. In this figure, vectors represent the u and v components of the flow field and colors represent the magnitude of local velocity, where blue areas represent stagnant flow regions. Figure 6
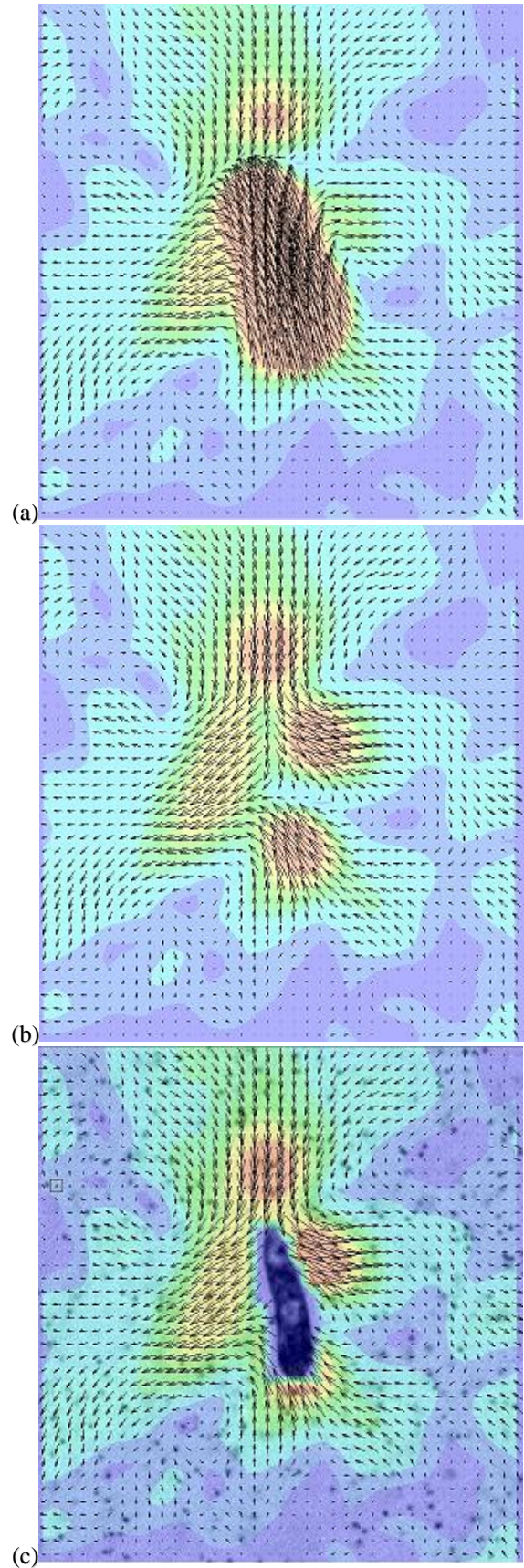

(a)

(b)

(c)

Figure 6. Flow field around *E. Gracilis* at t=1.92s. (a) Without masking, (b) with image masking only, and (c) with both image masking and vector masking. Max velocity is 12μm/s in b and c.

includes three subfigures in order to make a three way comparison of the flow field first without the application of masking (Fig. 6a), second with image masking but without vector masking (Fig. 6b), and third with both image and vector masking (Fig. 6c). The raw particle image is also included in Fig. 6c in order to show the position of *E. Gracilis* with respect to the flow field.

It is clear from Fig. 6a that without any masking the flow field in the immediate vicinity the organism is contaminated by the upward motion of the organism itself. This is simply because the features on the organism produce a strong correlation peak in interrogation areas that overlap the organism and the fluid around it. Application of image masking (Fig. 6b) improves the situation significantly for the liquid phase, but this time some erroneous vectors are registered on the organism; vectors indicate a downward motion while the organism swims upwards. These spurious vectors can be cleaned with the application of vector masking (Fig. 6c), which leaves us with the flow field around *E. Gracilis* where the information is only coming from the liquid phase. The flow field reveals that the fluid is drawn towards the organism upstream and downstream, and fluid is expelled from the organism on the sides. The downstream flow field can be explained as the wake in the aft of the swimmer, and the upstream flow field is produced most likely by the flagellum pulling a stroke, the main source of propulsion. Due to continuity around the organism, the fluid is expelled outwards from the sides. This flow field also produces four small vortices, one at each corner of the image, i.e. due Southwest, Southeast, Northwest and Northeast of the organism.

The histogram thresholding-based dynamic masking example described above proves to be quite powerful as it is able to tackle several important challenges encountered in the image ensemble: uneven illumination (Fig. 3a), random object trajectory, random object shape, and random object velocity (Fig. 4). Although quite powerful, histogram-thresholding based dynamic masking strategies may not work for certain applications. In the following section, the feature tracking-based dynamic masking strategy was used, which proved to be more successful for the application.

FEATURE TRACKING BASED DYNAMIC MASKING

Recently the hydrodynamics of a ~220-μm-long *A. Tonsa* (Fig. 7) nauplius were analyzed in Wadhwa et al. (2014) using time-resolved MicroPIV/PTV (Particle Tracking Velocimetry), in which a two-step masking technique was applied to remove the organism from the particle images.

Figure 7. Schematic of *A. Tonsa* nauplius at the beginning of a power stroke. From Ergin et al. (2015a).

vicinity of the organism, especially around the swimming appendages. As a result, Wadhwa et al. (2014) had to adjust the masking parameters for each recording manually in order to minimize the loss of useful data. Later Ergin et al. (2015a) made some improvements on the masking strategy of Wadhwa et al. (2014) and provided some phase-locked averaged results. In the current study, the same particle image ensemble is used, but a more effective approach for both masking and velocimetry is employed. Although the new strategy is not successful in masking the swimming appendages, it enables more accurate measurements in the close vicinity of the organism without having to adjust masking parameters manually for each image and without having to apply phase-locked averaging. In the current study, an improved tracking algorithm is used, which tracks both the horizontal and the vertical position of *A. Tonsa*, whereas, Ergin et al. (2015a) performed tracking only in the vertical direction. Since *A. Tonsa* is moving slightly to the left (see Fig. 11), a larger mask was used in Ergin et al. (2015a). Second, the analysis consists of 16x16 final IA size with 50% overlap followed by a UOD scheme with a detection threshold of 0.5. This enabled the comparison of masked and unmasked flow fields at any instant, without resorting to phase-locked averaging.

The experimental setup for the second application example is described in Wadhwa et al. (2014) and is summarized here briefly: Copepods *A. Tonsa* were cultured at 18°C and were transferred before experiments to the test aquarium containing filtered seawater. Only a few specimens were transferred in order to avoid possible interactions between them. The test aquarium is a glass cuvette (10x10x40mm) placed on a horizontal stage and kept at room temperature, between 18°C and 20°C.

The experimental measurement setup is a long-distance Micro Particle Image Velocimetry (LDμPIV) system where the light sheet propagation direction and the camera viewing direction are perpendicular. As described in the previous application, high-power visible laser illumination is often not preferred in biological
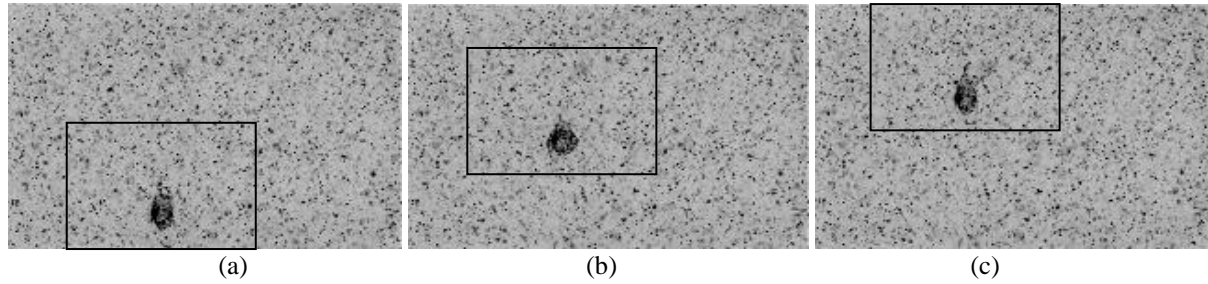
Figure 8. (a) First, (b) 33rd (middle), and (c) 65th (last) frames of the raw particle image ensemble. Boxes show the approximate borders of the ROI extracted around the organism.

flows. For this reason, a low-power, continuous-wave infrared laser (Oxford Lasers Ltd, 808nm wavelength) was used. Sheet forming optics were assembled to produce a 150μm thick light sheet, defining the measurement depth of the experiments. TiO_2 seeding particles smaller than 2μm were introduced in small quantities until a sufficient seeding density was achieved. The particle images were recorded on a high-speed CMOS detector (Phantom v210, Vision Research Inc.) at a resolution of 1280 x 800 pixels. Single frame image acquisition was performed with a constant time difference of 500μs between frames, corresponding to 2000fps. The images were acquired with 11.65x magnification producing a 2.2mm x 1.4mm FoV (approx $3mm^2$). Once again, the images were acquired and stored continuously in a ring buffer and the acquisition was stopped manually after the organism had passed through the FoV. Consecutive frames were used for two-frame PIV processing - quite typical for time-resolved PIV measurements: 65 frames were analyzed to produce 64 flow field measurements. Further details can be found in Ergin et al. (2015a).

The first, middle and last frame of the image ensemble are shown in Fig. 8, where a ~0.22mm tall *A. Tonsa* is in motion. During the experiment, *A. Tonsa* propels itself upwards through filtered seawater by pulling three breaststrokes and covering a distance of approximately 650μm (Average swim speed approx. 20mm/s). It is observed that *A. Tonsa* moves in an almost-vertical straight line and its angular orientation does not change significantly (Fig. 8 and 10). Subsequent image analysis includes feature tracking, image masking, velocity field calculation, vector masking and image masking.

Several different histogram thresholding-based dynamic masking strategies proved unsuccessful in a laboratory-fixed coordinate system; i.e. the "real-life" situation where the fluid is stationary and the microorganism is in motion. Since the microorganism did not rotate around its axis or change shape and moved in a relatively straight trajectory, a pixel-accurate, cross-correlation based tracking method was implemented in order to track its position throughout

the ensemble. The idea behind this tracking technique is to move to an object-fixed coordinate system in which the microorganism is fixed and the surrounding fluid is in motion. When the object is fixed, conventional static masking techniques can be applied on the images and/or on the calculated vectors. This was achieved in three steps: First, a feature was defined using the organism's image in the first frame (Fig. 8a). It was possible to identify the organism throughout the ensemble because some of the seeding particles were stuck on the organism (Fig. 9). For this reason, the tracked feature was selected as the body of the organism, excluding the appendages.

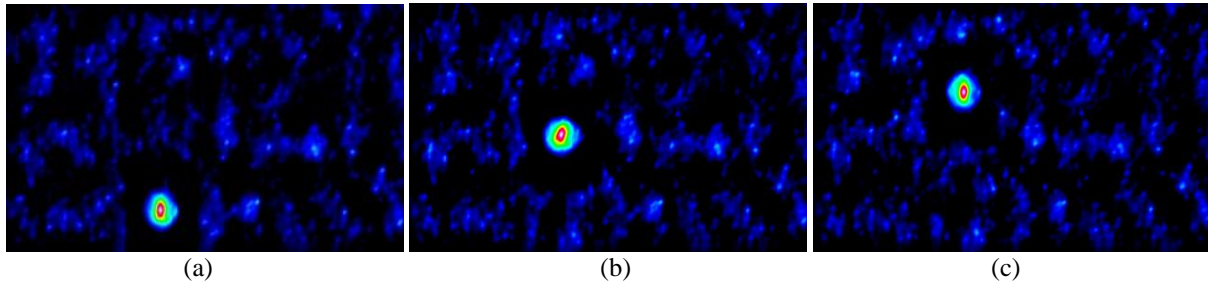**Figure 9.** Close up of the *A. Tonsa* showing particles stuck on its body.

70

Figure 10. Correlation of the organism with itself in the (a) first, (b) 33rd (middle), and (c) 65th (last) frames.

Second, a new pixel-accurate tracking algorithm was implemented in Matlab, which locates the peak of the cross-correlation function between the defined feature and the entire image (Fig. 8). This essentially searches for the defined feature within the entire image. The algorithm is only pixel accurate because no subpixel fitting was performed during the computations. Figure 10 shows the calculated cross correlation function for the first (Fig. 10a), the middle (Fig. 10b) and the last (Fig. 10c) frames in the ensemble, and the position of the cross correlation peak can be compared to the position of the organism in Fig 8a, 8b and 8c. The maximum pixel value of the cross correlation function in the ensemble reveals the nearly-linear trajectory of *A. Tonsa* (Fig. 11).
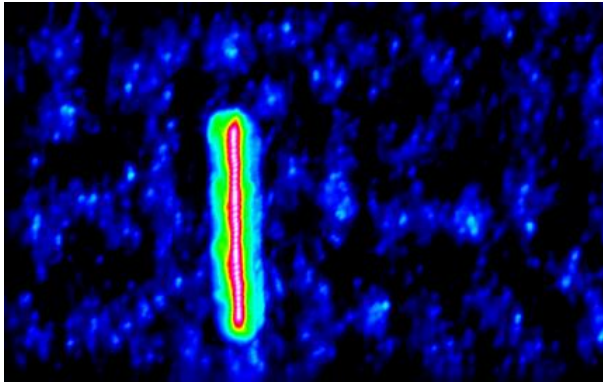

Figure 11. *A. Tonsa*'s nearly linear trajectory during the experiment.

Third, once the organism location was established on all frames, a constant-size ROI, (576x384 pix) was extracted around it (Fig. 8). The vertical ROI dimension (384 pixels) was the maximum value which could be used in all frames. The limitation was due to the first and the last frames, in which the imaged distance fore and aft of the organism must stay within the FoV throughout the ensemble (Fig. 8a and 8c). The horizontal ROI dimension (576 pixels) was a value which fixed the organism approximately in the center of the ROI horizontally, and reached sufficiently far into the flow field. This three-step procedure fixed the coordinate system on the organism and allowed the application of a conventional static masking procedure to remove the organism (image masking) and, eventually, the spurious vectors on the organism (vector masking). In this application, final interrogation windows of 16x16 pixel were used with 50% overlap for PIV processing. Here, the uncertainty of 0.055 pixels corresponds to a 94.4 nm displacement in the object space, and the velocity uncertainty is estimated as 189 μm/s; i.e. 1% compared to the average swim velocity. A flow chart describing the analysis chain for dynamic masking and PIV analysis of *A. Tonsa* is shown in Fig. 12.
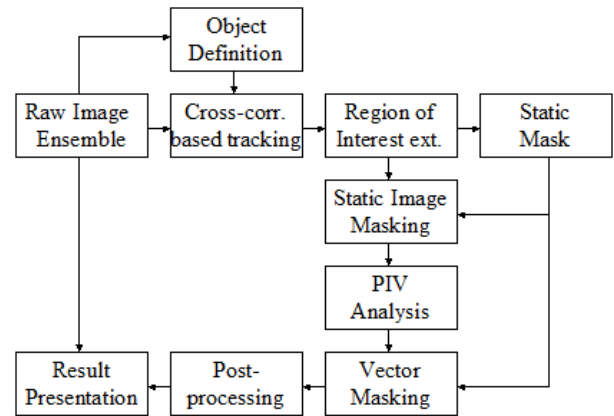

Figure 12. Flow chart describing the analysis chain for dynamic masking of *A. Tonsa*.

The organism's swim velocity history could be measured by probing a vector in the far field, upstream of or beside the organism. A time history of this vector showed that the nauplius is an almost perfectly periodic swimmer, and that three full breaststroke cycles were recorded (Ergin et al. 2015a). Figure 13 shows the flow field around the organism during the power stroke in the vicinity of the maximum swim speed. This figure includes two subfigures in order to make a comparison of the flow field without tracking and masking (Fig. 13a), and with tracking-based image and vector masking (Fig. 13b) at the same time instant. In Fig. 13b, the instantaneous swim velocity value is subtracted to show the flow field details around the organism. Similar to the case for *E. Gracilis*, it is clear from Fig. 13a that, without any masking, the flow field in the immediate vicinity of the organism is contaminated by the upward motion of the organism itself. This error is due to the fact that the features on the organism produce a strong correlation peak in interrogation areas which overlap both the organism and the fluid surrounding it. Application of image and vector masking (Fig. 13b) provides a cleaner picture where the flow field information around *A. Tonsa* is only extracted from the liquid phase.
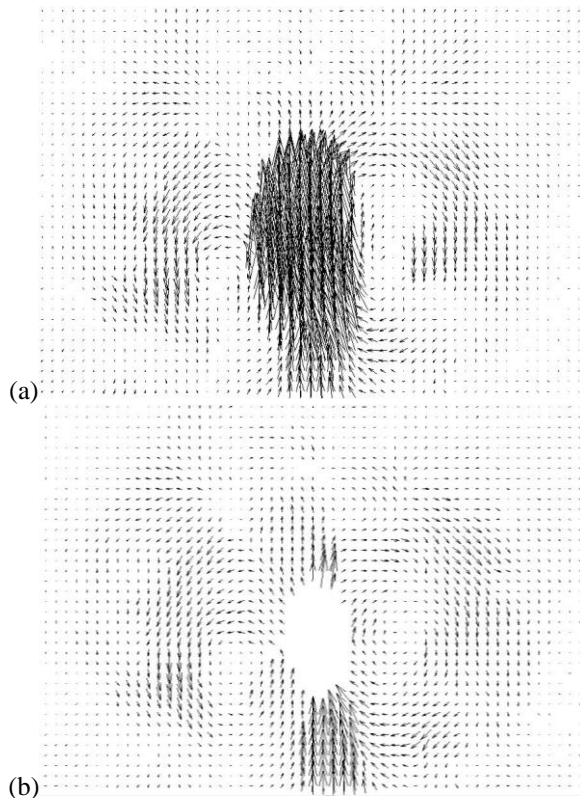
Figure 13. Flow field during the power stroke at t=3.5ms, (a) without masking (b) with image and vector masking. Swim speed at this instant is ~40mm/s. Both subfigures are a result of 16x16 final IA size, 50% overlap followed by UOD scheme with a detection threshold of 0.5.

In both masked and unmasked results, the wake behind the organism and two vortices are detected; one on each side of the organism and each with opposite rotation directions. The counter-rotating vortex system is an indication of a toroidal (ring) vortex system in three-dimensions which is in agreement with the previous findings in Wadhwa et al. (2014). The spatial dimension of the toroidal vortex is similar to the length of the organism. The observed toroidal vortex ring is more clearly visible in Fig. 13b when compared to Fig. 2 in Wadhwa et al. (2014). This is primarily due to the improved image processing functions used here. The masking process successfully removes the contribution of moving particles stuck on the organism.

DISCUSSION, RECOMMENDATIONS & FUTURE WORK

Masking will continue to be an important step in PIV analysis because it allows phase-separated measurements which improve the velocity accuracy along phase boundaries. Phase boundaries are locations where many interesting flow phenomena occur, such as velocity gradients, flow separations, gas expansions, impinging flows and many others. Ironically, this is where masking algorithms often fail and generate the most measurement uncertainty. This necessitates the evaluation of mask quality along the

actual phase boundaries and warrants some future investigations into the quantification of mask performance.

It was shown in both application examples that masking improves the accuracy and understanding of the flow field, by removing the swimming object from the analysis. Furthermore, it is shown in the case of *E. Gracilis* that vector masking should almost always be accompanied with image masking for a better representation of flow around the organism. It is described here as "a better representation" of the actual flow field, because the accuracy can still be improved. For instance, there are often sharp velocity gradients in thin boundary layers and the size of the interrogation window where the cross-correlation is applied is relatively large. In such situations, the displacement estimation is often biased towards the faster moving fluid particles which are located away from the wall in the correlation window. Vector repositioning, wall windowing or particle tracking techniques can further improve the accuracy close to these boundaries. Achieving improved accuracy using dynamic masking in conjunction with the above mentioned boundary techniques will be the subject of future investigations.

It is clear that the use of image processing functions is key for dynamic masking. Some image processing functions are more preferrable than others in the literature—median, opening, closing, erosion, dilation and threshold filters—and are widely used for histogram thresholding-based masking algorithms. Since the number of experimental conditions is infinite, it is essential to use these flexible image-processing functions to generate appropriate image masks. Additionally, manual mask generation is a user-dependent process and should be avoided if possible. Instead, masking should be performed based on algorithms in a systematic and traceable fashion. Another recommendation is to work with positive particle images during algorithm development, which can be achieved by a simple pixel inversion in cases with particle shadows.

Based on the results provided here, and in the author's opinion, a histogram thresholding-based dynamic masking is recommended if the object / surface is deforming and changing direction. On the other hand, feature tracking-based dynamic masking should be a better choice for dynamic masking if the object is rigid and does not rotate within the FoV. In practice, this is often not the case, because the object is either deforming or rotating. In order to cope with these situations, future investigations will focus on more advanced feature-tracking techniques where the tracked feature is changing shape and/or orientation from one frame to the next.

Currently, no automated dynamic masking technique is reported which is capable of working globally for every application. There is a general demand for a robust

technique that performs automatic object recognition and phase separation, both for double-frame and for time-resolved acquisitions. This warrants future investigations which focus on a hybrid technique (histogram thresholding + boundary detection + tracking) for automated dynamic masking with minimum input from the user. Edge detection methods are few and far between in the literature, which may indicate more possibilities for better algorithms. In particular, the actively deforming contours technique is interesting for investigation because of its applicability to both smooth and rough contours.

One final remark can be made on the effect of measurement plane thickness and object thickness on the accuracy of the masking techniques described here. (The thickness of the measurement plane is defined by the depth of field of the imaging system in the case for *E. Gracilis* and by the thickness of the light sheet in the case for *A. Tonsa*.) If the thickness of the object was much smaller than the measurement plane thickness, some particles may have been present in the illuminated zone between the object and the objective and could potentially be registered on the PIV images. This would have added some noise on top of the object image and may have had a negative influence on the accuracy for both masking techniques. Fortunately, in both dynamic masking applications presented here, the imaged objects are are thicker than the measurement plane, so noise-free object images were recorded.

ACKNOWLEDGMENTS

REFERENCES

Carrier O, Ergin FG, Li HZ, Watz BB and Funfschilling D "Time-resolved mixing and flow-field measurements during droplet formation in a flow-focusing junction" J. Micromech. Microeng. (2015) 15 084014

M1 - Movie of the droplet break-up experiment performed by Carrier et al. http://www.dantecdynamics.com/microfluidics-category/time-resolved-velocity-measurements-of-droplet-formation-in-a-flow-focusing-junction

Coron X, Champion JL and Champion M: Simultaneous measurements of velocity field and flame front contour in stagnating turbulent premixed flame by means of PIV. In 12th International Symposium on Applications of Laser Techniques to Fluid Mechanics, 2004.

Deen NG, et al. On image pre-processing for PIV of single-and two-phase flows over reflecting objects. Exp Fluids, 2010, 49.2: 525-530.

Ergin FG "Flow field measurements during microorganism locomotion using MicroPIV and dynamic masking" Proc. 11th Int. Symp. on PIV, Santa Barbara, California, September 14-16, 2015

Ergin FG, Watz BB and Wadhwa N "Pixel-accurate dynamic masking and flow measurements around small breaststroke-swimmers using long-distance MicroPIV" Proc. 11th Int. Symp. on PIV, Santa Barbara, California, September 14-16, (2015a)

Ergin FG, Watz BB, Erglis K and Cebers A "Time-resolved velocity measurements in a magnetic micromixer" Exp. Therm. Flu. Sci. (2015b) 67, pp. 6-13

Fritz HM, Hager WH and Minor HE "Landslide generated impulse waves. 1. Instantaneous flow fields" Exp Fluids 35 (2003) 505-519

Gui L and Merzkirch W (1996) Phase-separation of PIV measurements in two-phase flow by applying a digital mask technique. ERCOFTAC Bulletin 30: 45-48

Hammad KJ. "Liquid jet impingement on a free liquid surface: PIV study of the turbulent bubbly two-phase flow." In: ASME 2010 3rd Joint US-European Fluids Engineering Summer Meeting collocated with 8th International Conference on Nanochannels, Microchannels, and Minichannels. American Society of Mechanical Engineers, 2010. p. 2877-2885.

Honkanen M and Saarenrinne P "Multiphase PIV method with digital object separation methods" 5th International Symposium on PIV, Busan Korea, Sept 2003

Lindken R and Merzkirch W (2000) Velocity measurements of liquid and gaseous phase for a system of bubbles rising in water. Exp Fluids 29, 194-201

Lindken R and Merzkirch W (2002) A novel PIV technique for measurements in multiphase flows and its application to two-phase bubbly flows. Exp Fluids 33, 814-825

Sanchis A and Jensen A "Dynamic masking of PIV images using the Radon transform in free surface flows" Exp in Fluids 2011 51(4) 871-880

Seol DG and Socolofsky SA (2008) Vector post-processing algorithm for phase discrimination of two-phase PIV. Exp Fluids 45:223

Stevens EJ, Bray KNC and Lecordier B "Velocity and scalar statistics for premixed turbulent stagnation flames using PIV" Proc. 27th International Symposium on Combustion (1998) pp. 949-955.

Sveen JK and Dalziel SB "A dynamic masking technique for combined measurements of PIV and synthetic schlieren applied to internal gravity waves" Measurement Science and Technology, (2005) 16, 1954-1960

Wadhwa N, Andersen A and Kiørboe T "Hydrodynamics and energetics of jumping copepod nauplii and copepodids" J. Exp. Biol. (2014) 217, pp.3085-3094

Westerweel, J. and & Scarano, F. (2005). Universal outlier detection for PIV data. Experiments in Fluids, 39(6), 1096-1100.

Wosnik, M., and Arndt, R. E. A., (2013), "Measurements in High Void-Fraction Bubbly Wakes Created by Ventilated Supercavitation," ASME J. Fluids Eng. 135(1), pp. 011304-011304-9